Ca^{2+} dynamics in salivary acinar cells: distinct morphology of the acinar lumen underlies near-synchronous global Ca^{2+} responses

Olga Larina and Peter Thorn*

Department of Pharmacology, University of Cambridge, Tennis Court Road, Cambridge, CB2 1PD, UK
*Author for correspondence (e-mail: pt207@cam.ac.uk)

Accepted 9 June 2005
Journal of Cell Science 118, 4131-4139 Published by The Company of Biologists 2005
doi:10.1242/jcs.02533

Summary

In salivary acinar cells, the pattern of the Ca^{2+} signals that regulates fluid and enzyme secretion has yet to be resolved, as there are conflicting reports in the literature. We have used a two-photon technique to directly visualize the acinar cell lumen in living fragments of exocrine tissue and simultaneously recorded agonist-induced changes in intracellular Ca^{2+}. We show near-synchronous global Ca^{2+} responses in submandibular acinar cells, distinct from the typical apical to basal Ca^{2+} wave usually seen in rodent pancreatic acinar cells. In an effort to explain the basis of these near-synchronous global Ca^{2+} responses we used immunocytochemical experiments to localize luminal proteins and inositol trisphosphate receptors (InsP_3Rs) in tissue fragments. Zona occludens 1 (ZO-1), a tight junction protein, shows that individual submandibular acinar cells are often nearly completely encircled by a narrow luminal structure. By contrast, in pancreatic fragments, ZO-1 staining shows short luminal branches terminating abruptly at the apical pole of single acinar cells. Co-immunostaining of InsP_3Rs type 2 and type 3 showed them in the same region as ZO-1 in both exocrine tissues. Functional experiments showed that the near-synchronous global Ca^{2+} responses were still observed in the absence of extracellular Ca^{2+} and also in the presence of ryanodine. We conclude that the elaborate luminal region of submandibular cells leads to a hitherto unrecognized extensive distribution of InsP_3Rs in a band around the cell and that this underlies the near-synchronous global Ca^{2+} response to agonists. We suggest that this may be a structural adaptation in submandibular cells to support the copious amounts of fluid secreted.

Supplementary material available online at
http://jcs.biologists.org/cgi/content/full/118/18/4131/DC1

Key words: Acinar, Salivary gland, Calcium, Lumen

Introduction

The importance of intracellular Ca^{2+} in stimulus-secretion coupling in secretory epithelial cells has been long recognized (Matthews et al., 1973; Hunter et al., 1983; Petersen, 1992). The Ca^{2+} response is primarily the release of Ca^{2+} from intracellular stores and shows complex variations in time and space. Ca^{2+} oscillations in epithelia were first shown in parotid acinar cells (Gray, 1988) and since Kasai and Augustine's seminal paper on pancreatic acinar cells (Kasai and Augustine, 1990) an apical initiation and basal propagation of Ca^{2+} waves has become dogma in the field (Thorn et al., 1993; Toescu et al., 1992; Elliot et al., 1992; Lee et al., 1997). However, it is not clear if this is the case for salivary acinar cells where the patterns of Ca^{2+} signals in are still not resolved. Some report apical-to-basal Ca^{2+} waves are either not seen [parotid (Dissing et al., 1990)] or are very rapid, giving a near simultaneous Ca^{2+} response across the cell (Giovannucci et al., 2002; Takemura et al., 1999; Liu et al., 1998). By contrast, others report Ca^{2+} waves [submandibular (Lee et al., 1997; Harmer et al., 2005), parotid (Tojyo et al., 1997)] apparently similar to those seen in pancreatic acinar cells. A resolution of these different observations is essential to our general understanding of how Ca^{2+} signals are generated and how they regulate secretion.

There are two major problems with previous imaging studies of Ca^{2+} in polarized epithelia. Firstly, most use preparations of isolated cells, and small clusters of cells (<10 cells), where the characteristic morphology of polarized acinar cells is compromised because of the severing of tight junctions during cell isolation (Park et al., 2004). Secondly, the acinar lumen is not normally visible with light microscopy, so the apical domain is often identified simply as the region containing secretory granules. This distinction is functionally important; the luminal plasma membrane is the only region where exocytosis takes place and, in the generation of Ca^{2+} signals, inositol trisphosphate receptors (InsP_3Rs) are highly enriched, specifically in the endoplasmic reticulum immediately adjacent to the acinar lumen (Lee et al., 1997; Yule et al., 1997; Zhang et al., 1999).

We have overcome both of these problems using live-cell two-photon microscopy. Ca^{2+} responses from single cells, within large fragments of exocrine tissue that retain the morphological features of the intact gland (Park et al., 2004), were recorded with Fura-2. We visualized the ducts and acinar lumen by the simultaneous imaging of an extracellular fluorescent dye (Thorn et al., 2004).

Our experiments compare salivary and pancreatic tissue and

show that in submandibular acinar cells agonists evoke a near-synchronous Ca^{2+} rise across the cell comparable to the apical to basal Ca^{2+} waves seen pancreatic acinar cells. We show the acinar lumen in submandibular tissue is significantly more extensive than in pancreas, often leading to an encircling of single acinar cells with a band of InsP_3Rs. This hitherto unrecognized three-dimensional organization of InsP_3Rs explains the near-synchronous global Ca^{2+} signals in submandibular acinar cells, and the extensive luminal area is probably an adaptation in these cells that secrete copious amounts of fluid.

Materials and Methods

Cell preparation

Lobules and fragments (~50-100 cells) of mouse submandibular gland were prepared by collagenase digestion in normal Na^+-rich extracellular solution using the method of Thorn et al. (Thorn et al., 1993) modified to reduce the time in collagenase and limit mechanical trituration and cells were then plated onto poly-l-lysine-coated glass coverslips.

Na^+-rich extracellular solution contained (mM): 135 NaCl, 5 KCl, 1 $MgCl_2$, 10 Hepes, 10 glucose, 2 $CaCl_2$; pH 7.4. K^+-rich solution (mM): 5 NaCl, 135 KCl, 1 $MgCl_2$, 10 Hepes, 10 glucose, 2 $CaCl_2$; pH 7.4.

Immunofluorescence

Cells attached to glass coverslips were washed in PBS, fixed in methanol for 10 minutes at –20°C. After 1 hour in 2% donkey serum plus 2% fish skin gelatine in PBS, cells were incubated in primary antibody for 1 hour and then secondary antibodies for 30 minutes. The antibody dilutions were as follows: InsP_3R2 (pAb; Chemicon, Temecula, CA, USA), 1:20; InsP_3R3 (mAb; BD Transduction Laboratories, San Jose, CA, USA) 1:100; ZO-1 3 μg/ml (Zymed Laboratories Inc., San Francisco, CA, USA); AQP5 3 μg/ml (Alpha Diagnostic International Inc., San Antonio, TX, USA). The secondary antibodies used were Cy3-conjugated donkey anti-rabbit IgG (Jackson ImmunoResearch Laboratories Inc., USA; 1:200 dilution) and FITC-conjugated donkey anti-mouse IgG (Jackson ImmunoResearch Laboratories Inc., USA; 1:75 dilution), which showed no significant staining when applied alone. For the InsP_3R3 antibody, staining was abolished by preincubation with HeLa cell lysate containing the antigen.

Images were obtained on a Zeiss Axiovert LSM510 confocal microscope (Zeiss, Welwyn Garden City, UK), with a 63× oil immersion 1.4 NA objective. FITC was excited at 488 nm and emitted light captured through a 505-530 nm filter. Cy3 was excited at 543 nm and the emitted light captured through a 560 nm long-pass filter. Confocal image sections (z ~1 μm) were processed using Metamorph (Universal Imaging Corporation, Downington, PA, USA). The images in Figs 3 and 4 were obtained by a maximal projection of a stack of z sections taken through the acinus. Three-dimensional-rendered movies were created with Imaris (Bitplane Inc., St Paul, MN, USA).

Two-photon imaging

A Leica TCS MP, two-photon microscope with a 63× water immersion 1.2 NA objective, was used to collect images (resolution of 8-19 pixels/μm), which were analysed with Metamorph. Fura-2 regional kinetics were measured from regions of interest (16.9 μm^2). We observed no significant photobleaching; traces were rejected if movement was observed.

Ducts and the acinar lumen were imaged using either sulphorhodamine B (SRB; 500 μM) or Oregon Green 488 BAPTA-1 (OG; 100 μM) as membrane-impermeant extracellular markers. Dyes were excited at 740-780 nm, with fluorescence emission detected at 550-650 nm and <550 nm, respectively. Intracellular Ca^{2+} was monitored (emission of 490-540 nm) in cells loaded with Fura-2AM for 30 minutes at room temperature (~20°C). To normalize for differential Fura-2 dye distribution across the cell we obtained a pseudo-ratio (we termed self-ratio) by averaging the fluorescence for 20 frames prior to the response (F_0) and normalizing the subsequent fluorescence response according to the formula: F(pseudo ratio)=(F_0-F)/F_0). The Fura-2 images were all median filtered and displayed as pseudocolour images on an arbitrary blue-red scale using the programme ImageJ. The signal from the extracellular SRB fluorescence was binarized and shown as white on these images.

Fluorescent probes were from Molecular Probes Inc. (Eugene, OR, USA); all other compounds were from Sigma (Poole, UK).

Single-cell fluorescence measurements

Cell fragments, loaded with iIndo-1 AM for 30 minutes were washed, and plated onto coverslips. Single cells were illuminated (Nikon Diaphot inverted microscope, 40× oil immersion NA 1.3 objective) at 360 nm and emitted light collected at 410-430 nm and 430-600nm. The ratio of the two intensities was calibrated and expressed as Ca^{2+} concentration (Phocal, Strathclyde, UK).

Student's *t*-tests were used to test for significance and the probability (*P*) is quoted.

Results

Large volume changes in submandibular acinar cells

Lobules and fragments of exocrine tissue, loaded with Fura-2AM, were imaged on a two-photon microscope. With two photon excitation at 810 nm, elevated Ca^{2+} decreases Fura-2 emission measured at 490-540 nm (see Nemoto et al., 2001). Our experiments with pancreatic tissue showed large Fura-2 fluorescence decreases in response to acetylcholine (ACh), consistent with a Ca^{2+} rise. However, experiments with submandibular tissue often failed to show a decrease in Fura-2 fluorescence. We postulated that a reduction in cell volume, and subsequent concentration of dye, might be a major

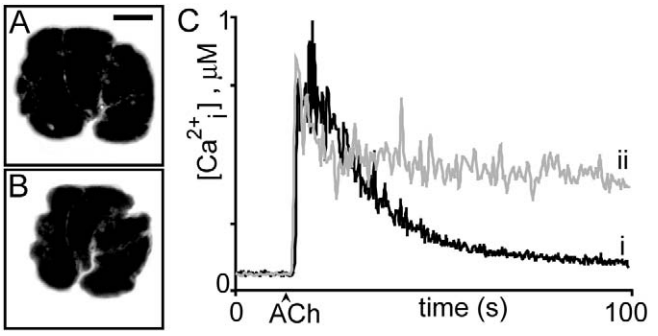

Fig. 1. Agonist-evoked shrinkage of submandibular acinar cells; effect of high extracellular K^+. A control cluster of submandibular acinar cells (A; approx. eight cells), washed in Na^+-rich extracellular medium containing the fluorescent dye, SRB and imaged with two-photon microscopy. (B) Fluorescent dye is excluded from the cell cytosol and dramatic decreases in cells volume in response to 10 μM ACh can readily be observed (B). (C) Superfusion with a K^+-rich extracellular solution (trace i, black) prevented cell swelling but had no effect on the early intracellular Ca^{2+} response to ACh compared with control (trace ii, grey) as measured in Indo-1 loaded cells. Scale bar: 10 μm.

problem in imaging submandibular acinar cells. To test this idea we used the two-photon microscope to image extracellular fluorescent dye (OG or SRB) and define the outside edge of cells (Fig. 1A). Apparent changes in cell volume were then determined assuming symmetrical cell dimensions. Stimulation of submandibular cells with 10 μM ACh (Fig. 1B) significantly decreased cell volume by 28.69±5.87% (mean±s.e.m., n=17, P<0.01). By contrast, ACh stimulation of pancreatic acinar cells did not produce a cell volume change (–0.24±0.84%, n=12, P=0.85; data not shown). To limit volume changes in submandibular cells we applied a K^+-rich extracellular solution; a condition expected to depolarize the cell and limit ion movements across the plasma membrane. Under these conditions the ACh-induced cell volume decrease in submandibular acinar cells was considerably attenuated; only a 6.54±1.71% decrease was observed (n=15).

The effect of K^+-rich extracellular solution on the Ca^{2+} signal was then determined in cells loaded with the ratiometric Ca^{2+}-sensitive dye Indo-1, a method chosen because the ratio is independent of changes in cell volume. We observed no significant difference in the peak Ca^{2+} response to 10 μM ACh (Fig. 1C, 0.69±0.15 μM n=10, in control; 0.75±0.25 μM, n=6 in K^+-rich solution, P=0.4). However, the plateau Ca^{2+}, measured at 300 seconds after the peak, was significantly smaller (0.21±0.03 μM, n=10 control; 0.10±0.01 μM in K^+-rich solution, n=9, P<0.01) consistent with cell depolarization reducing the driving force for Ca^{2+} entry. Since the initial Ca^{2+} response was unaffected, all subsequent experiments were carried out in K^+-rich solutions.

Near-synchronous global Ca^{2+} responses in submandibular acinar cells

Release of Ca^{2+} through InsP_3Rs is the major trigger for Ca^{2+} waves in acinar tissue. InsP_3Rs are found throughout the cell (Fogarty et al., 2000) but highly enriched in the endoplasmic reticulum adjacent to the luminal plasma membrane (Lee et al., 1997; Yule et al., 1997; Zhang et al., 1999). To identify the luminal region in living cells we added the fluorescent probe SRB to the extracellular media. The effective optical slice (~1 μm depth) of two-photon excitation enabled visualization of SRB fluorescence in the ducts and acinar lumen,

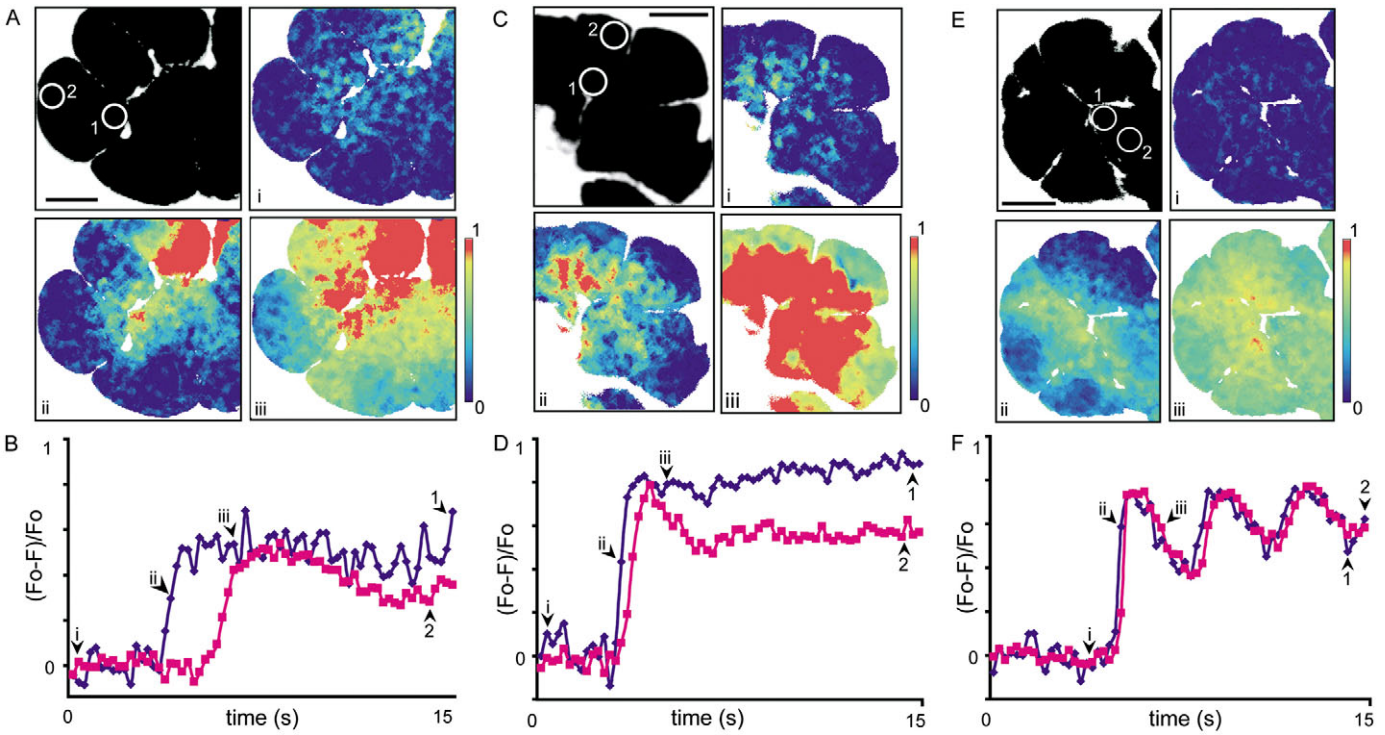

Fig. 2. Simultaneous identification of acinar lumens and agonist-evoked intracellular Ca^{2+} changes show near-synchronous global Ca^{2+} signals in submandibular acinar cells. Extracellular SRB fluorescence and intracellular Fura-2 fluorescence were recorded with two-photon microscopy to identify the acinar lumen and intracellular Ca^{2+} changes, respectively, in pancreatic fragments (10 μM ACh; A,B) and submandibular fragments (10 μM ACh C,D; 300 nM ACh; E,F). All Fura-2 self ratio images have been overlaid with a binary mask (in white) obtained from the SRB image. (A) In the top left panel, SRB outlines pancreatic acinar cells (image shows approx. seven cells on the edge of a tissue fragment) and fills the acinar lumens allowing placement of ROIs on the apical (ROI 1) and basal (ROI 2) pole of the cell. The pseudocolour images show ACh-induced Fura-2 self-ratio changes taken at the time points (i, ii, iii) shown on the graphs in B, which plot the average Fura-2 self-ratio changes over time in the ROIs. (C) In the top left panel, SRB outlines submandibular acinar cells (image shows approx. five cells on the edge of a tissue fragment). Acinar lumens are apparently elongated structures. ROIs were placed in the narrow, apparent apical pole of the cell (ROI 1) and wider, apparent basal (ROI 2) pole of the cell. The pseudocolour images show 10 μM ACh-induced Fura-2 self-ratio changes taken at the time points (i, ii, iii) shown on the graphs in D, which plot the average Fura-2 self-ratio changes over time in the ROIs. (E) In the top left panel, SRB outlines submandibular acinar cells (image shows approx. six cells on the edge of a tissue fragment). The pseudocolour images show 300 nM ACh-induced Fura-2 self-ratio changes taken at the time points (i, ii, iii) shown on the graphs in F, which plot the average Fura-2 self-ratio changes over time in the ROIs. Scale bars: 10 μm.

simultaneously with measurements of Fura-2 fluorescence inside acinar cells (Fig. 2A).

Within pancreatic fragments the acinar lumen, filled with fluorescent dye, appeared as a discrete region, usually close to the narrowest (apical) pole of the cell (Fig. 2A). Application of 10 μM ACh invariably led to a Ca^{2+} wave that was measured as the spread of the Ca^{2+} signal from a region of interest (ROI) placed adjacent to the acinar lumen to a ROI placed in a distant region in the basal pole (Fig. 2B, apparent wave velocity of 9.53±1.67 μm/second, n=30). By contrast, in submandibular fragments the acinar lumen often appeared as elongated regions not especially close to the narrow pole of the cell (Fig. 2C). ACh always elicited a Ca^{2+} response but obvious Ca^{2+} waves were not observed. Instead the Ca^{2+} signal in ROIs placed close to the apparent acinar lumen was nearly synchronous with those in ROIs placed on the opposite side of the cell (Fig. 2D, apparent wave velocity of 31.43±2.98 μm/second, n=39; significantly faster than the apparent wave velocity in pancreas P<0.01).

It has previously been shown in parotid acinar cells that the Ca^{2+} wave velocity slows at lower concentrations of agonist (Tojyo et al., 1997). This is probably due to a decrease in excitability when lower concentrations of InsP_3 are generated. It is therefore possible that submandibular acinar cells might generate more InsP_3 than pancreatic cells, through possession of either more cell-surface receptors or a more efficient signal cascade and this in turn might generate faster Ca^{2+} waves. We therefore tested the effects of lowered agonist concentrations in submandibular cells. In our hands 100 nM and 200 nM ACh rarely induced Ca^{2+} waves (2/15 cell clusters and 2/10 cell clusters, respectively). Although some cells did show noisy fluorescence signals, which might be indicative of localized Ca^{2+} responses as recently reported in submandibular cells (Harmer et al., 2005). At 300 nM ACh, Ca^{2+} waves were seen (9/15 cell clusters) and analysis of the responses showed an apparent Ca^{2+} wave velocity of 18.56±2.51 μm/second (n=29 cells, Fig. 2E,F). We conclude that even at a concentration of ACh that is threshold for inducing a Ca^{2+} wave, the apparent wave velocity in submandibular cells is still much faster (nearly double) than that in pancreatic acinar cells, consistent with a fundamental difference in the Ca^{2+} signalling machinery in the salivary cells.

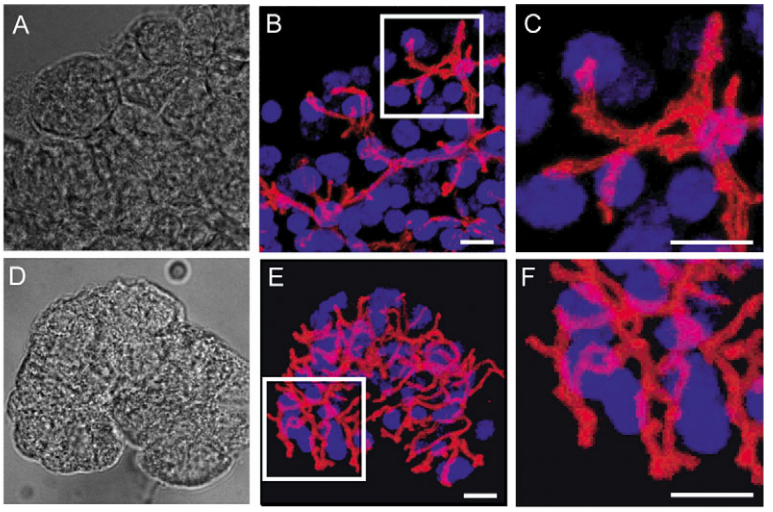

Fig. 3. ZO-1 staining of tissue fragments shows an extensive acinar lumen in submandibular cells. ZO-1 immunostaining (red, B,C,E,F) in pancreatic tissue fragments (A,B,C) and submandibular tissue fragments (D,E,F) counterstained with Hoechst 33258 (blue) to stain nuclei. (A,D) Phase-contrast images. The branching structure in B is shown in the magnified image in C to end abruptly at the narrow apical pole of pancreatic acinar cells. By contrast, an extensive lumen (E) is shown to encircle individual submandibular acinar cells (F). Images are projections of a series of z planes taken through the acinus. Scale bars: 10 μm.

The acinar lumen is highly elaborated in submandibular cells

SRB labelling of the acinar lumen suggested that submandibular tissue might have a much more extensive, luminal structure than that of pancreatic tissue.

Indeed early studies on salivary glands describe extensions to the main acinar lumen as intercellular canaliculi running between the cells with a morphology similar to the main acinar lumen (Tamarin and Sreebny, 1965). In subsequent studies intercellular regions were immunostained positive for InsP_3Rs and aquaporins (Lee et al., 1997; Matsuzaki et al., 1999; Takemura at al., 1999). However, these studies employed thin tissue sections in which three-dimensional structure is lost. To directly compare the luminal structures in pancreatic and submandibular tissue we therefore used tissue fragments that retain the three-dimensional structure of the intact gland. To identify the acinar lumen we immunostained for the tight junction protein zona occludens (ZO-1). In tissue fragments matched for the number of nuclei (stained with Hoechst 33258) we found a clear difference in the staining pattern of ZO-1 between the pancreas and the submandibular gland. In submandibular glands ZO-1 was much more extensively arborized compared with the simple branching structure found in the pancreas (Fig. 3A). Comparing magnified images of secretory endpieces, ZO-1 staining is apparent as a thin band (presumably, in reality, a tube) that in pancreatic tissue ends at a discrete region in one pole of the cells (Fig. 3B) but in submandibular tissue wraps around and almost completely encircles individual acinar cells (Fig. 3C,D). We quantified these differences, measuring the length of the terminal branches stained with ZO-1 (i.e. the last branch onto individual acinar cells). In pancreatic tissue branches were 6.44±0.35 μm in length (n=28), significantly shorter than branches in submandibular tissue, which were 11.67±0.64 μm (n=62) in length (P<0.01; see Movies 1 and 2 in supplementary material).

The elaborated acinar lumen in submandibular cells is enriched in InsP_3R

Our use of tissue fragments and three-dimensional reconstruction methods contrast the complexity of the elaborated lumens in submandibular tissue with the relatively simple structures found in the pancreas.

To test for differences in InsP_3R distribution we immunostained tissue fragments for InsP_3R-type 3 (InsP_3R3)

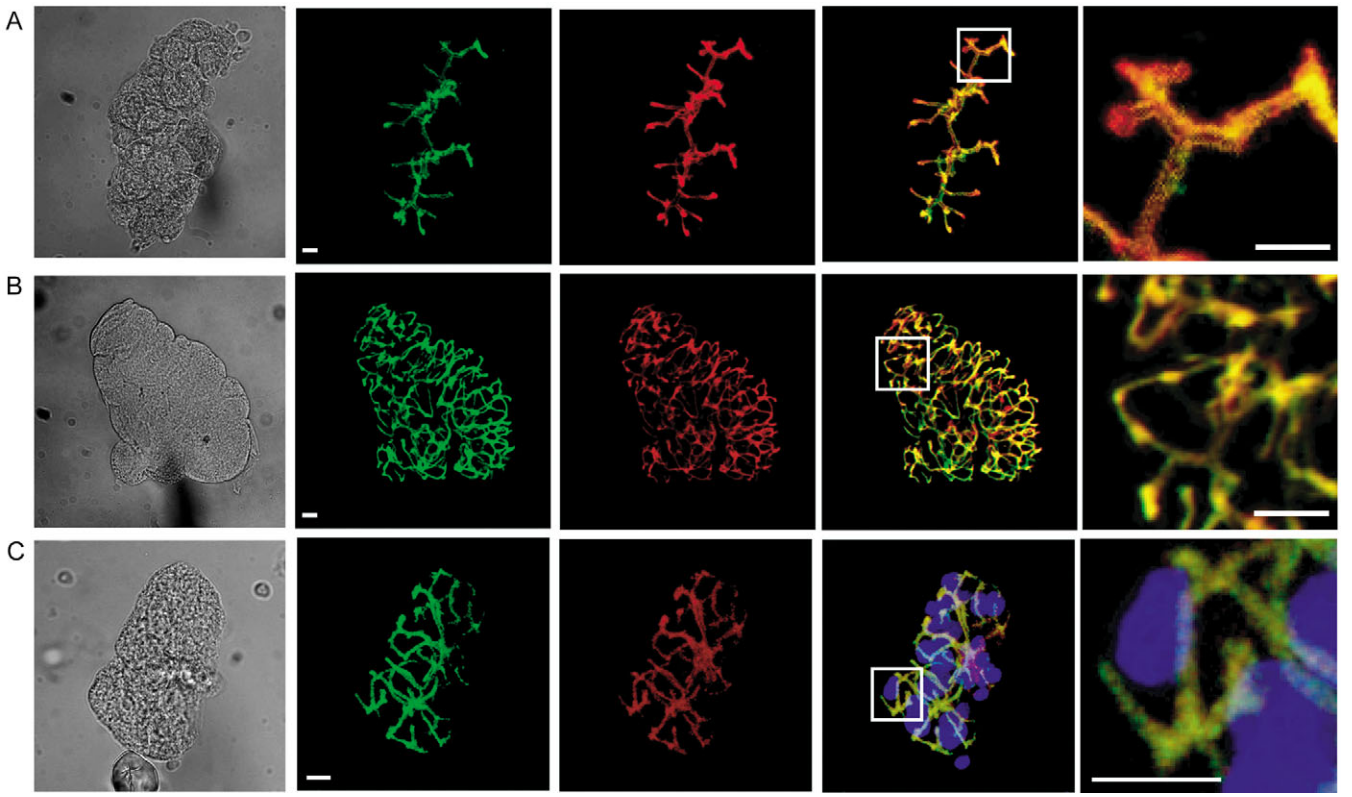

Fig. 4. InsP_3R3 and InsP_3R2 are closely associated with the acinar lumens in both pancreatic and submandibular acinar cells. ZO-1 immunostaining (red), Ins$P_3$3 immunostaining (green) are closely associated in pancreatic (A) and submandibular (B) tissue as observed in the overlay images (column 4) and in the magnified images (column 5). (C) In submandibular tissue InsP_3R3 (green) and InsP_3R2 (red) are also closely associated (overlay, column 4, magnified images, column 5) and apparently surround individual cells as shown by the nuclear Hoechst 33258 staining (blue). Images are projections of a series of z planes taken through the acinus. Column 1 shows the associated phase-contrast images. Scale bars: 10 μm.

and counter immunostained for ZO-1. Once again, submandibular cells (Fig. 4B) showed elaborate ZO-1 staining compared with that in pancreatic acinar cells (Fig. 4A). In both tissues immunostaining for InsP_3R3 localized closely with ZO-1 staining. InsP_3R2 is also present in salivary acinar cells (Lee et al., 1997; Takemura et al., 1999) and here we show that immunostaining for InsP_3R2 directly corresponds to immunostaining for InsP_3R3 (Fig. 4C).

This indicates that the whole length of the ZO-1 structures in both tissues is associated with InsP_3Rs. To determine if other luminal proteins are associated with ZO-1, we also immunostained for aquaporin-5 (AQP-5) (Matsuzaki et al., 1999), which was also found to follow the elaborated acinar lumens in submandibular cells (data not shown).

The near-synchronous global Ca^{2+} responses of submandibular cells are probably due to encircling of cells with InsP_3Rs

Since a band of InsP_3Rs nearly encircle submandibular acinar cells then this would provide an explanation for the near-synchronous Ca^{2+} increases across the cell. However, other possible explanations might include a role for Ca^{2+} influx. Ca^{2+} entry might be a larger component of the response in submandibular cells than in pancreatic acinar cells and as a consequence the Ca^{2+} wave might appear faster. However, two-photon experiments under the same conditions as shown in Fig. 2, but in the absence of extracellular Ca^{2+}, still showed a near-synchronous Ca^{2+} rise across the cell (Fig. 5A, Ca^{2+} wave velocity 24.30±3.85 μm/second, n=23).

Another possible difference is that ryanodine receptors (RYRs), thought to be present in acinar cells [submandibular (Lee et al., 1997), parotid (Zhang et al., 1999), pancreatic (Thorn et al., 1994)] may be differentially recruited in the two tissues. However, after pre-incubation of the cells in 20 μM ryanodine (RY), a concentration known to block RYRs, we still observed near-synchronous Ca^{2+} increases across the cell induced by the application of 10 μM ACh (Fig. 5B, apparent Ca^{2+} wave velocity 21.20±2.04 μm/second, n=52).

To further investigate a potential role for RYRs we conducted experiments with 200 mM ryanodine (observed apparent wave velocity 29.92±3.21 μm/second, n=18) and with ryanodine from another source (Tocris) at 20 μM (observed apparent wave velocity 30.94±2.81 μm/second, n=26) and 200 μM (observed apparent wave velocity 28.27±3.48 μm/second, n=16). In none of these experiments was there evidence for an action of ryanodine on the response induced by 10 μM ACh.

These experiments support the idea that it is the distribution of InsP_3Rs that underlies the faster wave velocities seen in submandibular cells.

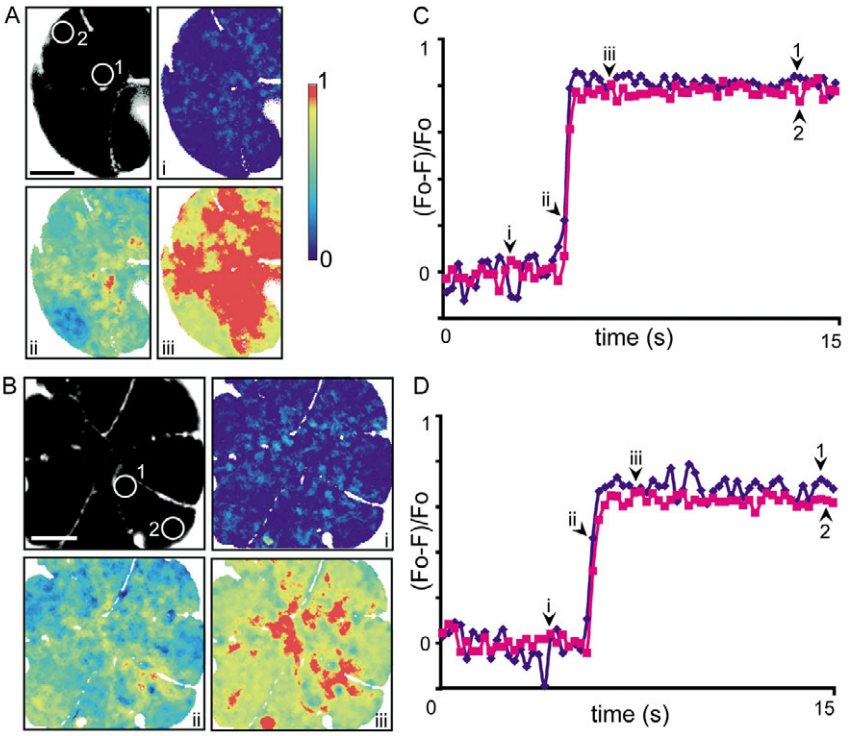

Fig. 5. Agonist-evoked intracellular Ca^{2+} changes in submandibular acinar cells are dependent on InsP_3Rs. Extracellular SRB fluorescence and intracellular Fura-2 fluorescence were recorded with two photon microscopy, as before, in submandibular fragments stimulated with 10 μM ACh in the absence of extracellular Ca^{2+} (A,C) and in the presence of ryanodine (B,D). All Fura-2 self-ratio images have been overlaid with a binary mask (in white) obtained from the SRB image. (A) In the top left panel, SRB outlines submandibular acinar cells (image shows approx. four cells on the edge of a tissue fragment) and fills the acinar lumens allowing placement of ROIs on the apical (ROI 1) and basal (ROI 2) pole of the cell. The pseudocolour images show ACh-induced Fura-2 self-ratio changes, in the absence of extracellular Ca^{2+}, taken at the time points (i, ii, iii) shown on the graphs in C which plot the average Fura-2 self-ratio changes over time in the ROIs. (B) In the top left panel, SRB outlines submandibular acinar cells (image shows three cells on the edge of a tissue fragment). ROIs were placed in the narrow, apparent apical pole of the cell (ROI 1) and wider, apparent basal (ROI 2) pole of the cell. The pseudocolour images show ACh-induced Fura-2 self-ratio changes, obtained in the presence of ryanodine, taken at the time points (i, ii, iii) shown on the graphs in D, which plot the average Fura-2 self-ratio changes over time in the ROIs. Scale bars: 10 μm.

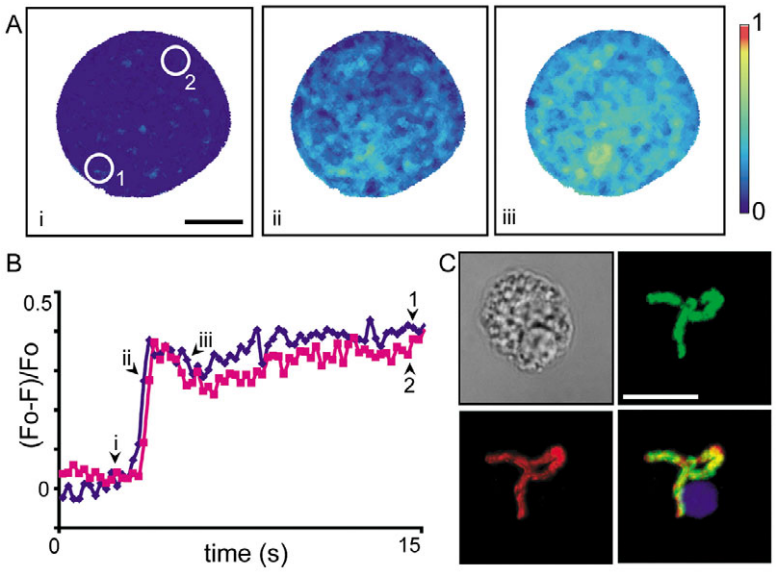

Fig. 6. Single submandibular cells show a decreased Ca^{2+} wave velocity compared with cells within a tissue fragment. Intracellular Fura-2 fluorescence was recorded with two-photon microscopy, as before, but in single isolated submandibular cells (A,B). All Fura-2 self-ratio images have been overlaid with a binary mask (in white) obtained from the SRB image. (A) The pseudocolour images show ACh-induced Fura-2 self-ratio changes taken at the time points (i, ii, iii) shown on the graphs in B, which plots the average Fura-2 self-ratio changes over time in ROI 1 and 2. (C) Immunocytochemistry shows ZO-1 (red) and InsP_3R3 (green) are still colocalized in these single cells (overlay also shows the nuclear Hoechst 33258 stain in blue). The phase-contrast image of the single cell is also shown. Scale bars: 10 μm.

Isolated single cells show slower apparent Ca^{2+} wave velocities

Our data is in contradiction to previous work on submandibular cells, in which slower Ca^{2+} wave velocities were recorded (Lee et al., 1997). One possible explanation is that previous studies often use single cells and clusters of small numbers of cells. To test for this possibility we measured Ca^{2+} responses from single submandibular cells. Our results showed Ca^{2+} responses to 10 μM ACh with an apparent Ca^{2+} wave velocity of 18.80±4.17 μm/second (n=15, Fig. 6). This is significantly slower than that recorded in tissue fragments, suggesting that the procedure used to isolate single cells may result in damage to the signal transduction machinery.

Discussion

Our imaging methods have allowed us to identify the acinar cell lumen in living exocrine tissue fragments and to simultaneously record acinar cell Ca^{2+} signal characteristics. In pancreatic tissue the lumen abuts the apical region of the cell and single acinar cells showed the typical agonist-evoked apical to basal Ca^{2+} waves. By contrast, in submandibular tissue the lumen was more extensive and was even found close to the apparent basal pole. In submandibular cells, agonists evoked near-synchronous global Ca^{2+} signals.

To investigate the basis of the differences in the Ca^{2+} signal between the two tissues we immunostained fixed tissue fragments. Immunostaining for the tight junction protein, ZO-1, defined the acinar lumen in pancreatic tissue as a branching system that terminates abruptly at the narrow apical pole of acinar cells. By contrast, in submandibular tissue ZO-1 immunostaining was much more extensive and single acinar cells were nearly encircled by a band of ZO-1 staining. These patterns of staining in the two tissues are entirely consistent with our live-cell two-photon imaging of the exocrine lumen with extracellular dyes. Immunostaining for InsP_3R2 and InsP_3R3 showed that both colocalize with ZO-1, as does AQP-5, indicating that the elaborated luminal structures of the submandibular acinar cells are probably of functional importance in generating the Ca^{2+} signal and in fluid secretion.

We show that the fast apparent Ca^{2+} wave velocity in submandibular acinar cells is retained in the absence of extracellular Ca^{2+} and also in the presence of ryanodine. These observations show that neither Ca^{2+} influx nor RYRs are important in the generation of the rapid global Ca^{2+} response and strongly implicate the more extensive distribution of InsP_3Rs in submandibular acinar cells as the fundamental factor in generating the fast Ca^{2+} wave. We conclude that the elaborated lumen and the near-encircling of the submandibular acinar cell with InsP_3Rs initiates the Ca^{2+} response at multiple sites around the cell, giving rise to a much higher apparent Ca^{2+} wave velocity than in the pancreas.

Comparative anatomy of the acinar lumen in submandibular and pancreatic tissue

Two independent lines of evidence, imaging of extracellular dyes and immunostaining of ZO-1, show a much more extensive acinar lumen in submandibular than in pancreatic tissue. This data is absolutely consistent with observation of intercellular canaliculi in salivary acinar cells that have been reported previously (Tamarin and Sreebny, 1965; Matsuzaki et al., 1999). However, to our knowledge, no direct comparative studies across different exocrine tissues has previously been performed, and it is this side-by-side comparison of submandibular with pancreatic tissue that highlights the contrasting anatomy of the two exocrine glands. These differences are further highlighted in our study through our use of 3D reconstruction techniques (see Fig. 4 and Movies 1 and 2 in supplementary material) where the near-encircling of submandibular acinar cells with InsP_3Rs is immediately apparent in a way not obvious in single thin sections.

Ca^{2+} wave velocity measurements

The dramatic tissue-type differences we see in Ca^{2+} wave velocity (9.5 μm/second in pancreatic and 31.4 μm/second in submandibular tissue) are consistent with most previous reports (Thorn et al., 1992; Giovannucci et al., 2002; Takemura et al., 1999; Liu et al., 1998; Tojyo et al., 1997). In other reports, slower Ca^{2+} waves were seen in submandibular tissue (Lee et al., 1997; Harmer et al., 2005). In Harmer et al.'s (Harmer et al., 2005) study this may be due to the relatively high imposed Ca^{2+} buffering in their patch-clamp experiments (500 μm EGTA plus 100 μm Fura-2) which would tend to slow wave velocities (see Kidd et al., 1999) and in Lee et al.'s (Lee et al., 1997) study it may be due to the use of small clusters of acinar cells, which we show does slow Ca^{2+} wave speeds (Fig. 6).

What underlies the higher apparent Ca^{2+} wave velocity in salivary acinar cells?

Giovannucci et al. (Giovannucci et al., 2002) have explicitly investigated tissue differences between pancreatic and parotid glands. They showed that the parotid gland acinar cell Ca^{2+} response was more sensitive than the pancreas cells to small increases in InsP_3 concentration: low concentrations of InsP_3 that induced local Ca^{2+} responses in pancreatic acinar cells induced global Ca^{2+} responses in the parotid acinar cells. They suggested that these differences might be due to different levels of InsP_3R expression and showed that the parotid gland contained fourfold more InsP_3Rs, as measured by radioligand binding and western blotting experiments than the pancreas (Giovannucci et al., 2002). This data is entirely consistent with our own observations. It is likely that the extended distribution of InsP_3Rs we report in salivary glands, distributed along the extended acinar lumen, requires the higher levels of receptor expression seen by Giovannucci et al. (Giovannucci et al., 2002).

However, alone, these lines of evidence do not directly link InsP_3R number and distribution with the differences in the Ca^{2+} response between pancreatic and salivary acinar cells. What we have done is to directly demonstrate that neither Ca^{2+} influx nor possible Ca^{2+} release from RYR-sensitive Ca^{2+} stores can explain the fast Ca^{2+} wave in submandibular cells. Since RYRs are known to be present in salivary acinar cells (Lee et al., 1997; Zhang et al., 1999) it might be expected that they do play a role. However, we have previously shown in pancreatic acinar cells that ryanodine is most effective in blocking the Ca^{2+} responses induced by low agonist concentrations (Thorn et al., 1994). This presumably is a circumstance where relatively modest levels of InsP_3 only partially recruit the InsP_3R pool and where the total Ca^{2+} response may depend on a parallel recruitment of RYRs. By contrast, at high agonist concentrations, sufficient InsP_3 is generated to recruit the total InsP_3R pool and the majority of the Ca^{2+} response will therefore be derived from the InsP_3Rs. Whatever the explanation, ryanodine, even at the extremely high concentration of 200 μM, failed to affect the Ca^{2+} response of submandibular cells (Fig. 5) and we can conclude that the differences in the Ca^{2+} signal between the pancreas and submandibular acinar cells are therefore most probably dependent on the different distributions of the InsP_3Rs.

What we are actually observing when we measure Ca^{2+} wave velocities is not clear. The measured Ca^{2+} wave velocity is much higher than would be expected by simple Ca^{2+} diffusion. These high velocities are therefore likely to be a reflection of either the regenerative spread of Ca^{2+} along InsP_3Rs by the positive feedback process of Ca^{2+}-induced Ca^{2+}-release (CICR active on InsP_3Rs) or the temporally coordinated release of Ca^{2+} from InsP_3Rs. It is not clear which mechanism dominates the response in submandibular cells, but in either case it is the distribution of InsP_3Rs that would be critical to shaping of the Ca^{2+} signal.

Physiological relevance

In terms of the physiological response, the rodent pancreatic acinar cell is thought to have a relatively poor fluid secretory output (Argent et al., 1986) compared with the submandibular acinar cell (Foskett et al., 1989). This is shown in our measurements of cell volume changes, which directly reflect ion movements during the first stages of fluid secretion. Here we show significant changes in volume in submandibular cells but not in pancreatic cells, indicating a greater ion flux in the salivary tissue [see Fig. 1, and also Foskett (Foskett, 1990)]. Fluid secretion is, in the first instance, instigated by the opening of apical Cl^- channels but activation of a K^+ channel is required to maintain cell hyperpolarization and to provide a route for K^+ exit (Petersen, 1992; Hayashi et al., 1995; Takeo et al., 1998). Salivary acinar cells have a robust Ca^{2+}-dependent K^+ conductance (Maruyama et al., 1983; Smith and Gallacher, 1992) and the fact that this is missing in rodent pancreatic acinar cells (Kidd and Thorn, 2001) may explain their weaker secretory response. The identity of the Ca^{2+}-dependent K^+ channel, recruited during fluid secretion in salivary acinar cells, is not known (Hayashi et al., 1995) but most models of secretion would place the K^+ channel on the basal plasma membrane. This positioning is supported by the work of Harmer et al. (Harmer et al., 2005), which does show evidence that the Cl^- current can, at low levels of cell stimulation, be activated alone. However, much work on salivary acinar cells shows a nearly simultaneous activation of K^+ and Cl^- current on cell stimulation (Foskett et al., 1989; Takeo et al., 1998). This might arise because of an apical location of K^+ channels, but our work suggests an alternative hypothesis. Unlike the classical view, derived from the pancreatic acinar cells, where the basal plasma membrane can be some distance from the discrete apical region, we show that in submandibular acinar cells the luminal region encircles the cells and thus the basal plasma membrane is actually close to the apical domain. We would therefore expect that the extended luminal region associated with an extended area of InsP_3Rs would rapidly active luminal Cl^- channels but the near-synchronous global Ca^{2+} responses that arise from this distribution of InsP_3Rs would also trigger the rapid activation of Ca^{2+}-dependent K^+ channels even if they were exclusively in the basal plasma membrane. Further work will be required to directly compare fluid secretion in pancreatic and submandibular tissues and test these ideas.

Conclusions

In conclusion, our data show an extended acinar lumen in submandibular glands nearly encircles individual acinar cells and is associated with a characteristic near-synchronous global Ca^{2+} response. We speculate that these are important adaptations to support copious fluid secretion in these cells.

This work was funded by a Wellcome Trust Overseas Fellowship to O.L. and Medical Research Council (UK) project grants (G0000214, G0400669 to P.T.). We thank Ian Parker for help with the movies.

References

Argent, B. E., Arkle, S., Cullen, M. J. and Green, R. (1986). Morphological, biochemical and secretory studies on rat pancreatic ducts maintained in tissue culture. *Q. J. Exp. Physiol.* **71**, 633-648.

Dissing, S., Nauntofte, B. and Sten-Knudsen, O. (1990). Spatial distribution of intracellular, free Ca^{2+} in isolated rat parotid acini. *Pflügers Arch.* **417**, 1-12.

Elliott, A. C., Cairns, S. P. and Allen, D. G. (1992). Subcellular gradients of intracellular free calcium concentration in isolated lacrimal acinar cells. *Pflügers Arch.* **422**, 245-252.

Fogarty, K. E., Kidd, J. F., Tuft, R. A. and Thorn, P. (2000). Mechanisms underlying $InsP_3$-evoked global Ca^{2+} signals in pancreatic acinar cells. *J. Physiol.* **3**, 515-526.

Foskett, J. K. (1990). $[Ca^{2+}]_i$ modulation of Cl^- content controls cell volume in single salivary acinar cells during fluid secretion. *Am. J. Physiol.* **259**, C998-C1004.

Foskett, J. K., Gunter-Smith, P. J., Melvin, J. E. and Turner, R. J. (1989). Physiological localization of an agonist-sensitive pool of Ca^{2+} in parotid acinar cells. *Proc. Natl. Acad. Sci. USA* **86**, 167-171.

Giovannucci, D. R., Bruce, J. I. E., Straub, S. V., Arreola, J., Sneyd, J., Shuttleworth, T. J. and Yule, D. I. (2002). Cytosolic Ca^{2+} and Ca^{2+}-activated Cl^- current dynamics: insights from two functionally distinct mouse exocrine cells. *J. Physiol.* **540**, 469-484.

Gray, P. T. (1988). Oscillations of free cytosolic calcium evoked by cholinergic and catecholaminergic agonists in rat parotid acinar cells. *J. Physiol.* **406**, 35-53.

Harmer, A. R., Smith, P. M. and Gallacher, D. V. (2005). Local and global calcium signals and fluid and electrolyte secretion in mouse submandibular cells. *Am. J. Physiol.* **288**, G118-G124.

Hayashi, T., Hirono, C., Young, J. A. and Cook, D. I. (1995). The ACh-induced whole-cell currents in sheep parotid secretory cells. Do BK channels really carry the ACh-evoked whole-cell K^+ current? *J. Memb. Biol.* **144**, 157-166.

Hunter, M., Smith, P. A. and Case, R. M. (1983). The dependence of fluid secretion by mandibular salivary gland and pancreas on extracellular calcium. *Cell Calcium* **4**, 307-317.

Kasai, H. and Augustine, G. J. (1990). Cytosolic Ca^{2+} gradients triggering unidirectional fluid secretion from exocrine pancreas. *Nature* **348**, 735-738.

Kidd, J. F. and Thorn, P. (2001). The properties of the secretagogue-evoked chloride current in mouse pancreatic acinar cells. *Pflügers Arch.* **441**, 489-497.

Kidd, J. F., Fogarty, K. E., Tuft, R. A. and Thorn, P. (1999). The role of Ca^{2+} feedback in shaping $InsP_3$-evoked Ca^{2+} signals in mouse pancreatic acinar cells. *J. Physiol.* **520**, 187-201.

Lee, M. G., Xu, X., Zeng, W., Diaz, J., Wojcikiewicz, R. J. H., Kuo, T. H., Wuytack, F., Racymaekers, L. and Muallem, S. (1997). Polarized expression of Ca^{2+} channels in pancreatic and salivary gland cells. Correlation with initiation and propagation of $[Ca^{2+}]_i$ waves. *J. Biol. Chem.* **272**, 15765-15770.

Liu, P., Scott, J. and Smith, P. M. (1998). Intracellular calcium signalling in rat parotid cells that lack secretory vesicles. *Biochem. J.* **330**, 847-852.

Maruyama, Y., Gallacher, D. V. and Petersen, O. H. (1983). Voltage and Ca^{2+}-activated K^+ channel in baso-lateral acinar cell membranes of mammalian salivary glands. *Nature* **302**, 827-829.

Matsuzaki, T., Suzuki, T., Koyama, H., Tanaka, S. and Takata, T. (1999). Aquaporin-5 AQP5), a water channel protein, in the rat salivary and lacrimal glands: immunolocalization and effect of secretory stimulation. *Cell Tissue Res.* **295**, 513-521.

Matthews, E. K., Petersen, O. H. and Williams, J. A. (1973). Pancreatic acinar cells: acetylcholine-induced membrane depolarization, calcium efflux and amylase release. *J. Physiol.* **234**, 689-701.

Nemoto, T., Kimura, R., Ito, K., Tachikawa, A., Miyashita, Y., Iino, M. and Kasai, H. (2001). Sequential-replenishment mechanism of exocytosis in pancreatic acini. *Nat. Cell Biol.* **3**, 253-258.

Park, M. K., Lee, M. and Petersen, O. H. (2004). Morphological and functional changes of dissociated single pancreatic acinar cells: testing the suitability of the single cell as a model for exocytosis and calcium signalling. *Cell Calcium* **35**, 367-379.

Petersen, O. H. (1992). Stimulus secretion coupling: cytoplasmic calcium signals and the control of ion channels in exocrine acinar cells. *J. Physiol.* **448**, 1-51.

Smith, P. M. and Gallacher, DV. (1992). Acetylcholine- and caffeine-evoked repetitive transient $Ca(^{2+})$-activated K^+ and $C1^-$ currents in mouse submandibular cells. *J. Physiol.* **449**, 109-120.

Takemura, H., Yamashina, S. and Segawa, A. (1999). Millisecond analysis of Ca^{2+} initiation sites evoked by muscarinic receptor stimulation in exocrine acinar cells. *Biochem. Biophys. Res. Comm.* **259**, 656-660.

Takeo, T., Suga, S., Wu, J., Dobashi, Y., Kanno, T. and Wakui, M. (1998). Kinetics of Ca^{2+} release evoked by photolysis of caged $InsP_3$ in rat submandibular cells. *J. Cell Physiol.* **174**, 387-397.

Tamarin, A. and Sreebny, L. M. (1965). The rat submaxillary salivary gland. A correlative study by light and electron microscopy. *J. Morphol.* **117**, 295-352.

Thorn, P., Lawrie, A. M., Smith, P. M., Gallacher, D. V. and Petersen, O. H. (1993). Local and global cytosolic Ca^{2+} oscillations in exocrine cells evoked by agonists and inositol trisphosphate. *Cell* **74**, 661-668.

Thorn, P., Gerasimenko, O. and Petersen, O. H. (1994). Cyclic ADP-ribose regulation of ryanodine receptors involved in agonist evoked cytosolic Ca^{2+} oscillations in pancreatic acinar cells. *EMBO J.* **13**, 2038-2043.

Thorn, P., Fogarty, K. E. and Parker, I. (2004). Zymogen granule exocytosis is characterized by long fusion pore openings and preservation of vesicle lipid identity. *Proc. Natl. Acad. Sci. USA* **101**, 6774-6779.

Toescu, E. C., Lawrie, A. M., Petersen, O. H. and Gallacher, D. V. (1992). Spatial and temporal distribution of agonist-evoked cytoplasmic Ca^{2+} signals in exocrine acinar cells analysed by digital image microscopy. *EMBO J.* **11**, 1623-1629.

Tojyo, Y., Tanimura, A. and Matsumoto, Y. (1997). Imaging of intracellular Ca^{2+} waves induced by muscarinic receptor stimulation in rat parotid acinar cells. *Cell Calcium* **22**, 455-462.

Turvey, M. R. and Thorn, P. (2004). Lysine-fixable dye tracing of exocytosis shows F-actin coating is a step that follows granule fusion in pancreatic acinar cells. *Pflügers Arch.* **488**, 552-555.

Turvey, M. R., Fogarty, K. E. and Thorn, P. (2005). Inositol 1,4,5-trisphosphate receptor links to filamentous actin are important for generating local Ca^{2+} signals in pancreatic acinar cells. *J. Cell Sci.* **118**, 971-980.

Yule, D. I., Ernst, S. A., Ohnishi, H. and Wojcikiewicz, R. J. H. (1997). Evidence that zymogen granules are not a physiologically relevant calcium pool. *J. Biol. Chem.* **272**, 9093-9098.

Zhang, X., Wen, J., Bidasee, K. R., Besch, H. R., Jr, Wojcikiewicz, R. J., Lee, B. and Rubin, R. P. (1999). Ryanodine and inositol trisphosphate receptors are differentially distributed and expressed in rat parotid gland. *Biochem. J.* **340**, 519-527.